ISCI, Volume *11*

Supplemental Information

Ultrathin Nanosheet of Graphdiyne-Supported Palladium Atom Catalyst for Efficient Hydrogen Production

Huidi Yu, Yurui Xue, Bolong Huang, Lan Hui, Chao Zhang, Yan Fang, Yuxin Liu, Yingjie Zhao, Yongjun Li, Huibiao Liu, and Yuliang Li

Supplemental Information

Supplemental Figures

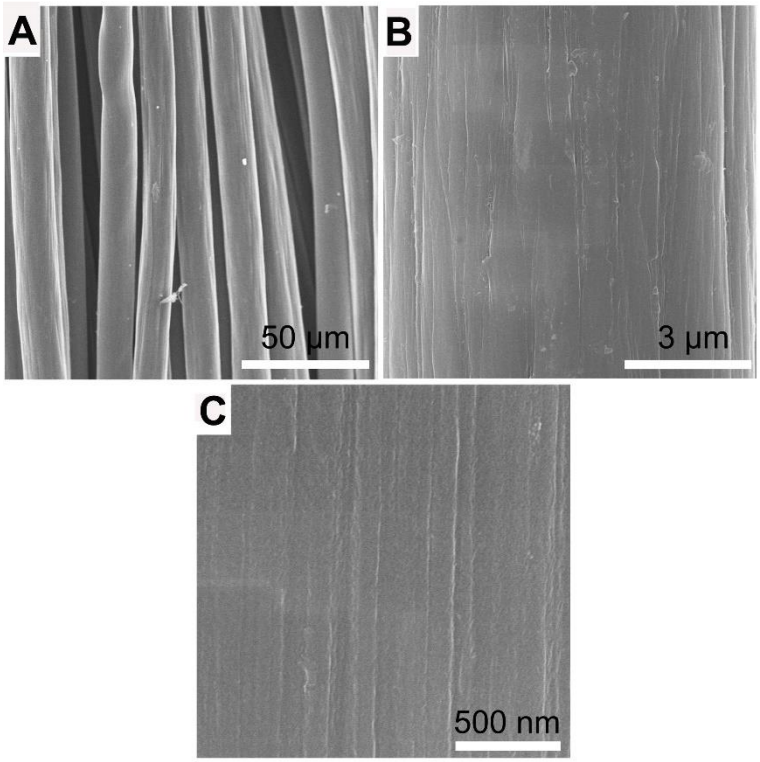

Figure S1. Morphology characterization of CF, related to Figure 3.

(A-C) SEM images of CF in different magnifications. The morphology of smooth CF surface is clearly shown.

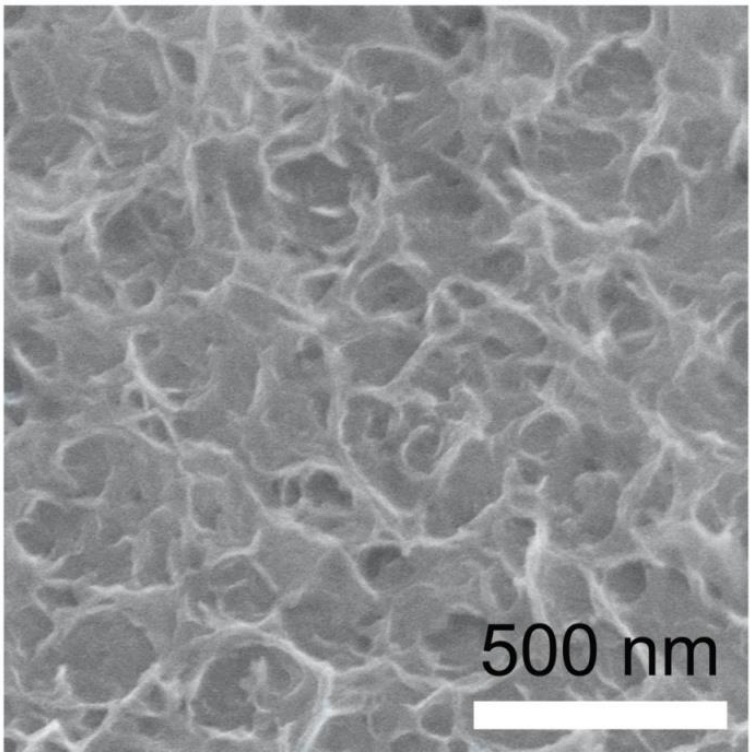

Figure S2. Morphology characterization of GDY, related to Figure 3.

SEM image of pristine GDY.

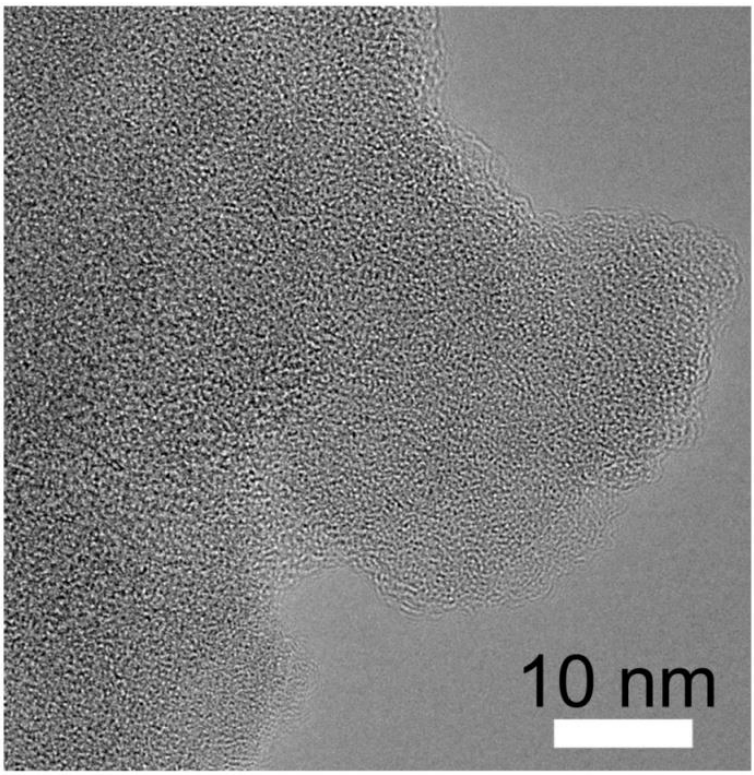

Figure S3. Characterization of GDY, related to Figure 3.

TEM image of the pristine GDY nanosheet.

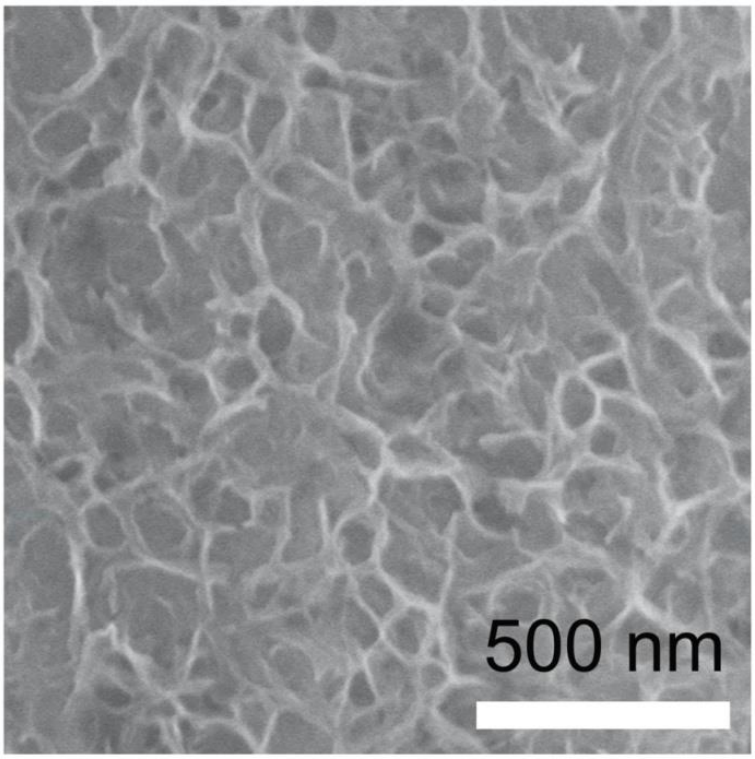

Figure S4. Morphology characterization of Pd^0/GDY, related to Figure 3.

SEM image of Pd^0/GDY, confirming the preservation of nanosheet structure.

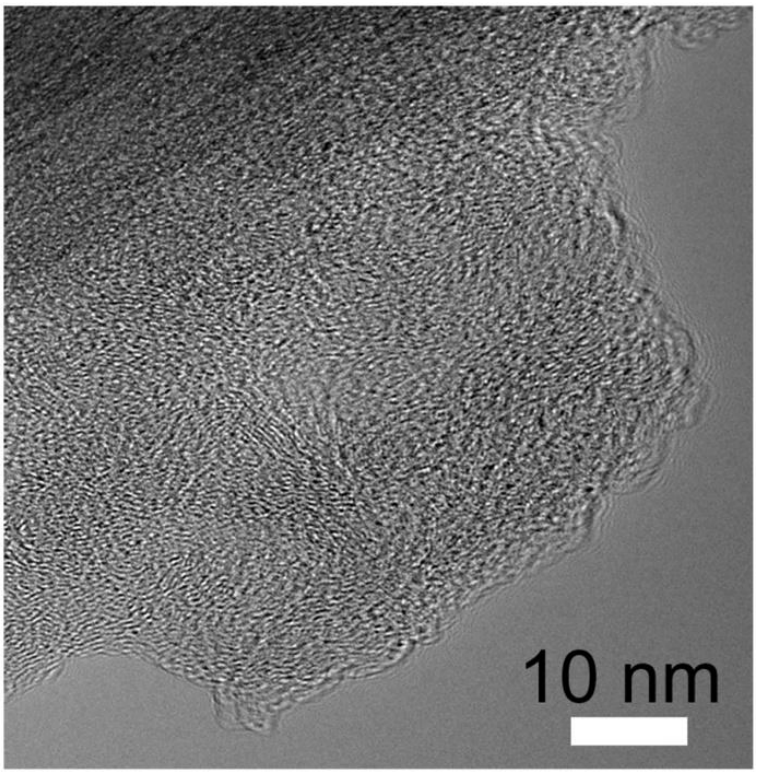

Figure S5. Characterization of Pd^0/GDY, related to Figure 3.

TEM image of Pd^0/GDY, indicating the absence of aggregated Pd nanoparticles.

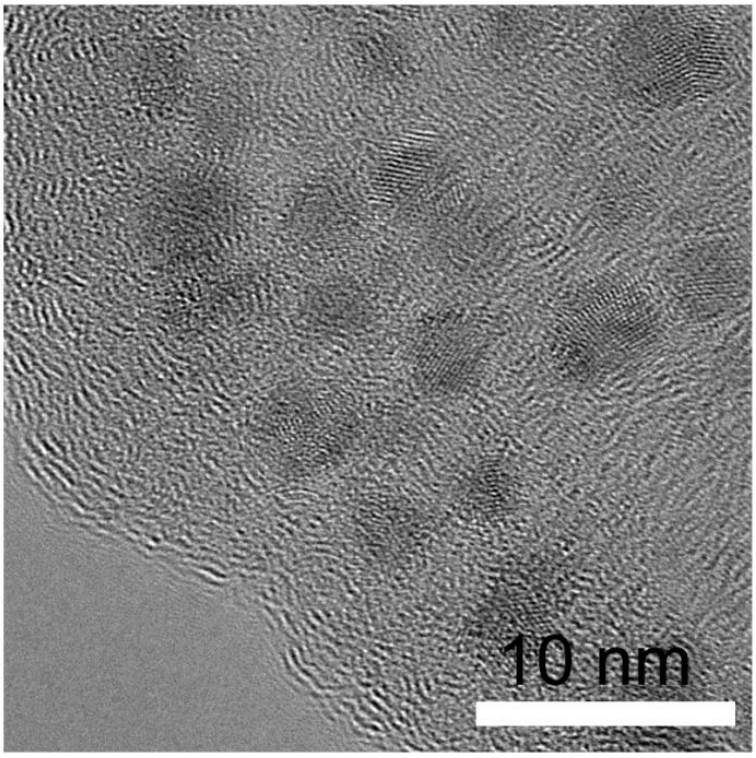

Figure S6. Characterization of Pd NP/GDY, related to Figure 3.

The high-resolution TEM image of Pd NP/GDY, demonstrating the successful deposition of Pd nanoparticles onto GDY substrate.

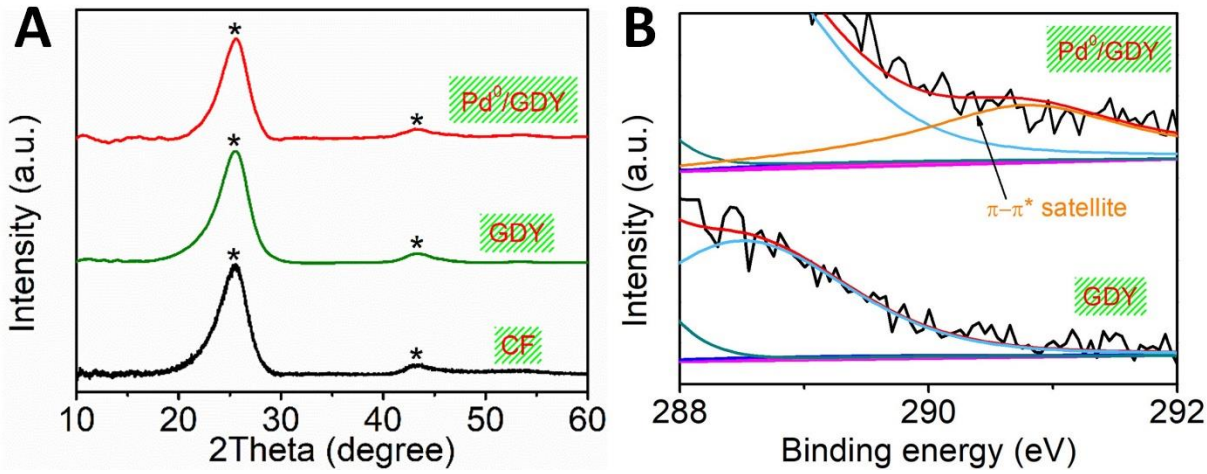

Figure S7. Structural analysis of the as-synthesized samples, related to Figure 5.

(A) XRD patterns of Pd^0/GDY, GDY and CF. The peaks marked with * represent the characteristic peaks of carbon species. No characteristic peaks of Pd species can be observed in Pd^0/GDY. (B) The magnified images of the C 1s at 290.8eV region of Pd^0/GDY and the pristine GDY.

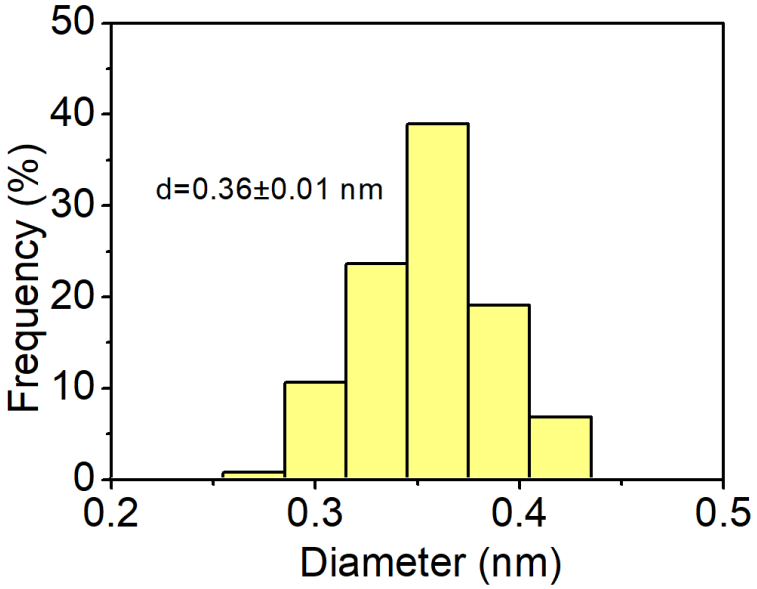

Figure S8. Size distribution, related to Figure 4.

Size distribution of Pd atoms of Pd^0/GDY. The Pd atom size is precisely measured and analyzed from HAADF images of Pd^0/GDY.

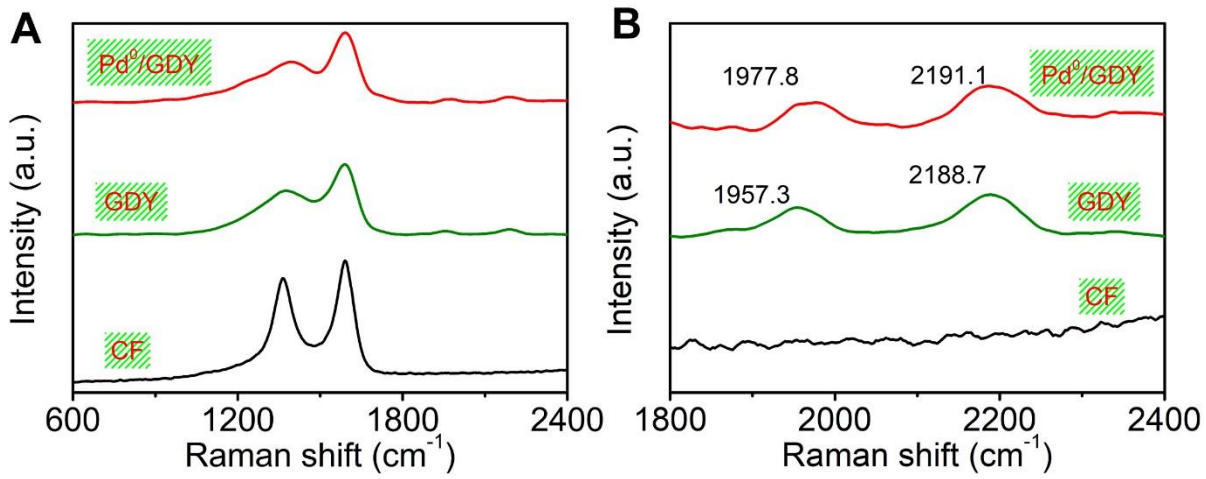

Figure S9. Raman spectra of the catalysts, related to Figure 5.

(A) The Raman spectra of Pd^0/GDY, GDY and CF. (B) The Raman spectra of Pd^0/GDY, GDY and CF within Raman shift from 1800 to 2400 cm^{-1}.

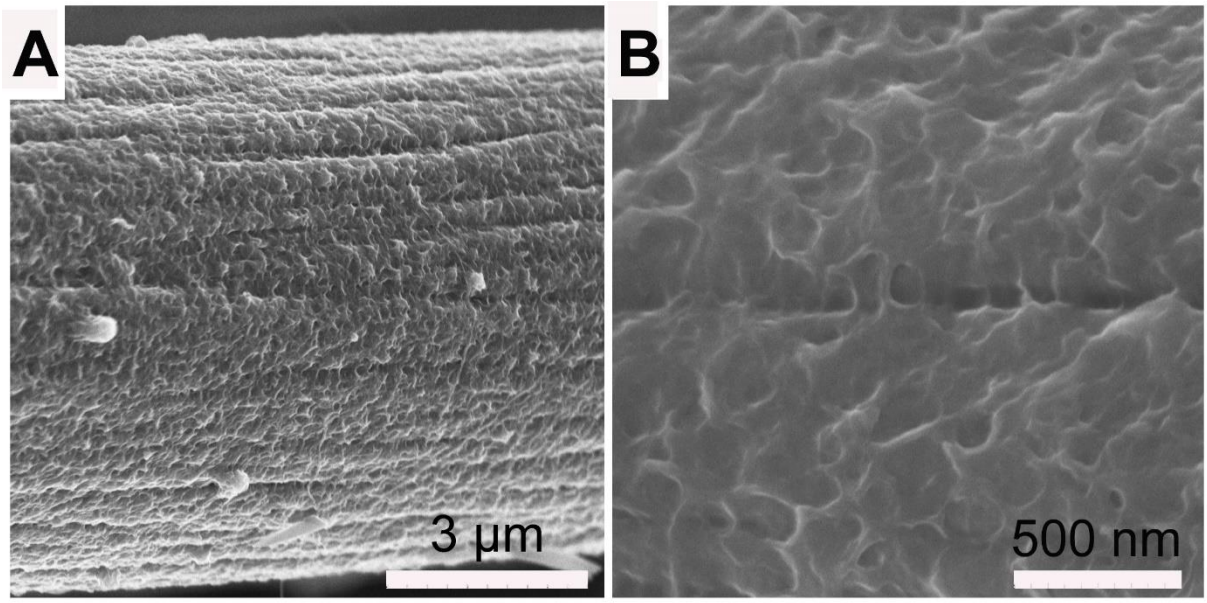

Figure S10. SEM images of Pd^0/GDY after CV cycles, related to Figure 6.

(A) The SEM image of Pd^0/GDY loaded on a single carbon fiber; (B) Magnified image from A.

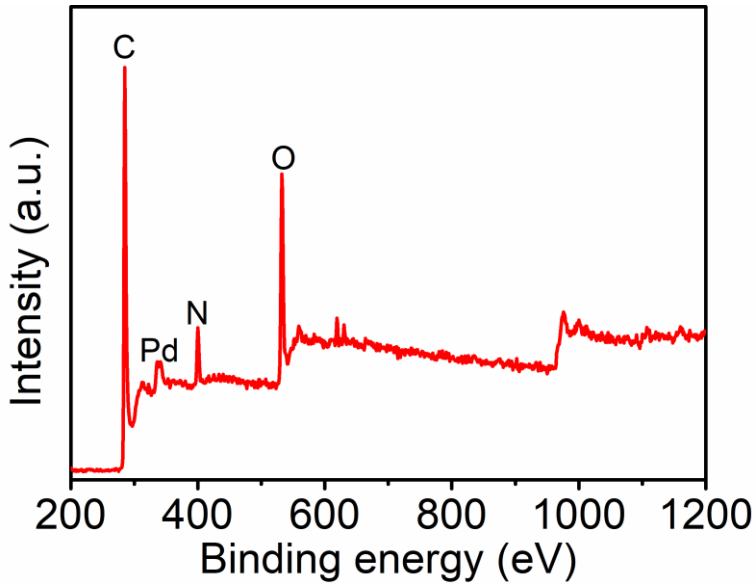

Figure S11. XPS survey spectrum of Pd^0/GDY, related to Figure 6.

XPS survey spectrum of Pd^0/GDY after CV cycles. All the elements remain identical with the sample before CV, indicating the preservation of element composition of Pd^0/GDY.

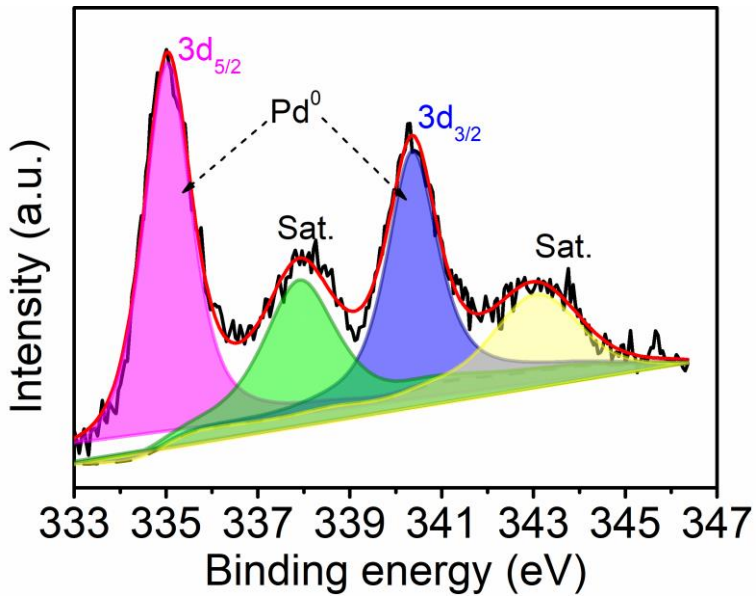

Figure S12. XPS Pd 3d spectrum of Pd^0/GDY after CV cycles, related to Figure 6.

XPS Pd 3d spectrum of Pd^0/GDY after CV cycles. The deconvoluted $3d_{5/2}$ (335.0) and $3d_{3/2}$ (340.4) peaks indicated that Pd remained in its metallic state, confirming the valence reliability of Pd^0/GDY electrocatalyst.

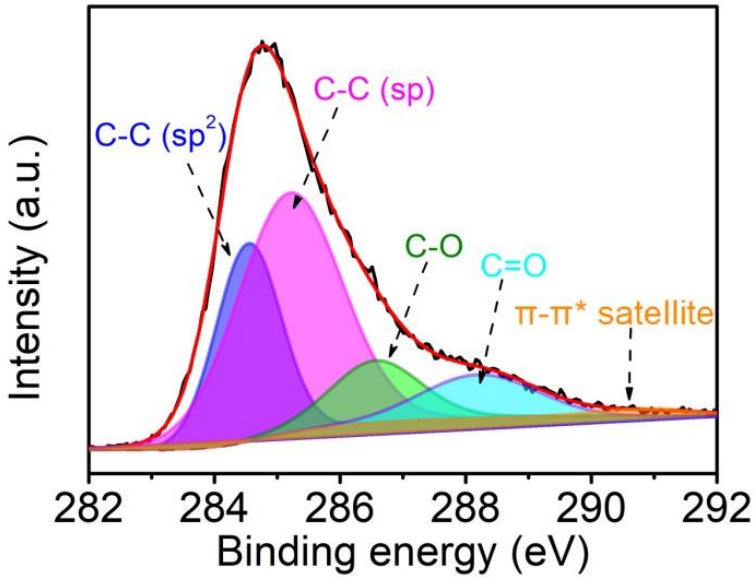

Figure S13. XPS C 1s spectrum of Pd^0/GDY after CV cycles, related to Figure 6.

XPS C 1s spectrum of Pd^0/GDY after CV cycles. Deconvolution indicated the presence of sp-C (285.2 eV), sp^2-C (284.5 eV), C-O (286.6 eV), C=O (288.2 eV) and π-π* transition (290.9 eV), demonstrated the maintained structure and chemical state of GDY network.

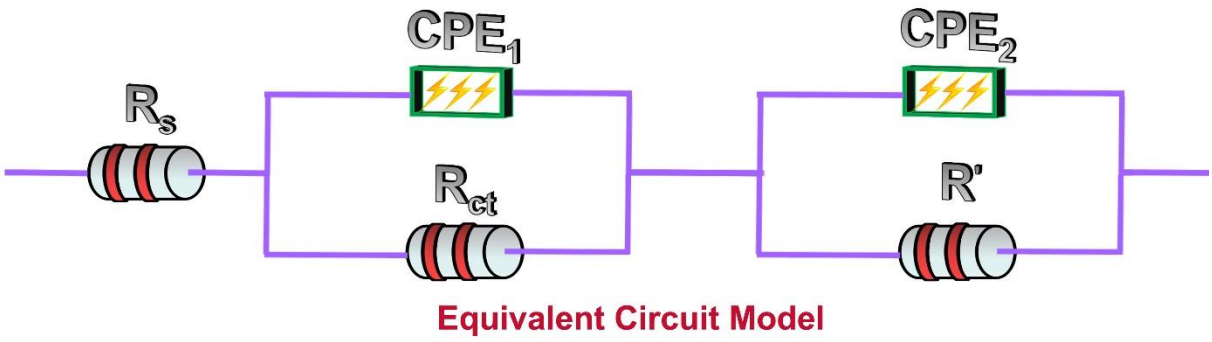

Figure S14. An equivalent circuit model, related to Figure 6.

The R(QR)(QR) equivalent circuit model for fitting and analyzing EIS data.

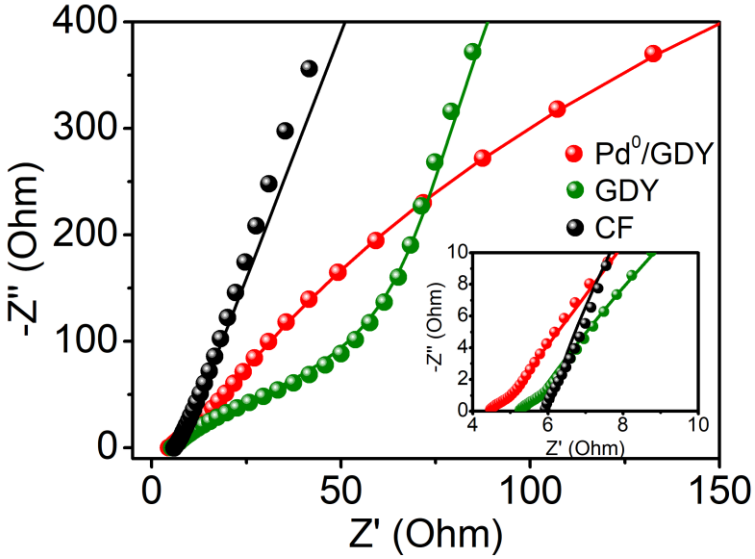

Figure S15. Electrochemical impedance spectroscopy results, related to Figure 6.

The fitted image for EIS data. The spheres represent the experimental Nyquist plots, while the lines with corresponding colors are the fitted results. The inset is the corresponding EIS data in low frequency. The analyzed data fit well with the original experimental EIS data.

Supplemental Tables

Table S1. Comparison of the HER performance of Pd^0/GDY with traditional single-atom catalysts in 0.5 M H_2SO_4, related to **Figure 6**.

Catalysts	**Mass loading (mg cm^{-2})**	**Metal loading**	**η_{onset} (mV)**	**$\eta_{10\ mA\ cm^{-2}}$ (mV)**	**Tafel slope (mV dec^{-1})**	**Stability (cycles)**	**Reference**
Pd^0/GDY	**0.207**	**0.2%**	**11**	**55**	**47**	**1000**	**This work**
$Mo_1N_1C_2$	0.408	1.32%	48	154	86	1000	*Angew. Chem. Int. Ed.* **56,** 16086 (2017)
Co-NG	0.285	0.57%	30	147	82		*Nat. Commun.* **6,** 8668 (2015)
ALDPt/NGNs	N/A	2.1%		ca.60	29	1000	*Nat. Commun.* **7,** 13638 **(**2018**)**
Fe/GD	N/A	0.680%	9	66	37.8	5000	*Nat. Commun.* **9,** 1460 (2018)
Ni/GD	N/A	0.278%		88	45	5000	*Nat. Commun.* **9,** 1460 (2018)
Pt–MoS_2	0.018	1.7%		ca.160	96	5000	*Energy Environ. Sci.* **8,** 1594 (2015)
Co_9S_8/1L MoS_2	N/A	N/A		95	71	1000	*Adv. Mater.* **30,** 1707301 (2018)
Pt1@Fe-N-C	0.4	2.1%		60	42		*Adv. Energy Mater.* **8,** 1701345 (2018)
Fe-N_4 SAs/NPC	N/A	1.96%		202	123		*Angew. Chem. Int. Ed.* **57,** 8614 (2018)

Table S2. Comparison of the HER performances of Pd^0/GDY with benchmarked bulk catalysts in 0.5 M H_2SO_4, related to **Figure 6**.

Catalysts	**Mass loading (mg cm^{-2})**	**η_{onset} (mV)**	**$\eta_{10\ mA\ cm^{-2}}$ (mV)**	**Tafel slope (mV dec^{-1})**	**Stability (cycles)**	**Reference**
Pd^0/GDY	**0.207**	**11**	**55**	**47**	**1000**	**This work**
PtO_x/TiO_2	N/A		ca.140	40	3000	*Energy Environ. Sci.* **10,** 2450 (2017)
$Co_{0.97}V_{0.03}SP$	0.28	23	55	50		*Adv. Energy Mater.* **8,** 1702139 (2018)
core–shell CoP@PS/NCNT	N/A		80	53	1000	*Adv. Energy Mater.* **8,** 1702806 (2018)
N-WC nanoarray	16		89	75		*Nat. Commun.* **9,** 924 (2018)
BP/Co_2P	0.14	105	ca.250	62		*Angew. Chem. Int. Ed.* **57,** 2600 (2018)
N@$MoPC_x$-800	0.14	32	108	69.4	1000	*Adv. Energy Mater.* **8,** 1701601 (2018)
Ni_2P@NPCNFs	N/A	52	63.2	56.7	3000	*Angew. Chem. Int. Ed.* **57,** 1963 (2018)
G@N-MoS_2	0.25		243	82	1000	*Adv. Mater.* **30,** 1705110 (2018)

Table S3. The fitted EIS parameters, related to **Figure 6.**

Catalysts	**R_s (Ω)**	**CPE_1 (S sec^n)**	**n_1**	**R_{ct} (Ω)**	**CPE_2 (S sec^n)**	**n_2**	**R' (Ω)**
Pd^0/GDY	4.549	1.127×10^{-4}	0.9497	3.367	3.623×10^{-4}	0.793	4.422×10^{4}
GDY	5.303	2.175×10^{-4}	0.8213	30.97	1.552×10^{-4}	0.8513	1.508×10^{5}
CF	6.103	3.84×10^{-6}	0.9707	54.37	3.282×10^{-6}	0.8567	1.08×10^{10}

Transparent Methods

Materials

Tetrabutylammonium fluoride (TBAF) was purchased from Alfa Aesar. Hexabromobenzene was brought from J&K Scientific. Toluene and tetrahydrofuran (THF) were refluxed with sodium pieces for sufficient time in order to remove the remaining water. All other reagents were purchased from Sinopharm Chemical Reagent Co., Ltd., and used without further purification unless specifically mentioned. The water used for all experiment was purified with a Millipore system. All the chemicals were of chemical grade and were used as received without further purification.

Preparation of GDY

GDY was synthesized following the previously reported method with minor modification. Several pieces of copper foil and commercial carbon cloth (CC) were added into a three-necked flask containing 100 mL pyridine. The reactor was kept at 110 ^{o}C for 2 hours for the adequate release of catalytic active Cu(I) ions and its sufficient adsorption onto CC. Subsequently, 30 mg HEB was dissolved in 50 mL pyridine and added very slowly into the above flask. The cross-coupling reaction proceeded in the protection of Ar atmosphere at 110 C^{o} in dark. After 3 days, the CC loaded with GDY nanosheet was move out and cleaned with hot acetone and DMF, then thoroughly cleaned with KOH (4 M), HCl (6 M), KOH (4 M) and deionized water in sequence to get rid of the residual copper. The 3D flexible GDY substrate was successfully obtained for the preparation of ACs and subsequent electrochemical tests.

Preparation of Pd^0/GDY

The as prepared GDY substrate was fixed on an electrode clip as working electrode, together with a graphite counter electrode and a saturate calomel reference electrode to establish a three electrode system. The electrochemical deposition was conducted by immersing the GDY electrode into $PdCl_2$ solution (0.2 mM; 0.5 M H_2SO_4 as solvent) and immediately subject to galvanostatic conditions at a current density of 2 mA cm^{-2} for 10 s using an electrochemical workstation (CHI. 660D, Shanghai CH. Instruments, China). The Pd^0/GDY was successfully prepared and washed with H_2SO_4 (0.5 M), deionized water and H_2SO_4 (0.5 M) sequentially, then used for electrochemical measurements immediately. The Pd NP/GDY was synthesized using the electrochemical deposition method. Briefly, the as prepared GDY substrate was used as working electrode, together with a graphite counter electrode and a saturate calomel reference electrode to establish a three electrode system. The GDY electrode was immersed into $PdCl_2$ solution (1.0 mM; 0.5 M H_2SO_4 as solvent) and immediately subject to galvanostatic conditions at a current density of 2 mA cm^{-2} for 100 s. The obtained sample was washed thoroughly using H_2SO_4 (0.5 M) and used for electrochemical measurements immediately.

Calculation setup

We performed the density functional theory (DFT) calculations based on the CASTEP code (Clark et al., 2005). For the electronic orbital potential projection calculations, the related calculations are carried out by recently developed ab-initio orbital self-energy minimization technique (Huang., 2016; Huang., 2016; Huang., 2017; Huang., 2016). This method provides the detail of the self-consistent determination process for the orbital parameters with best matching the specific chemical bonding environment of the given solid materials systems. The on-site electronic orbital negativity induced potential and screened pseudo-charge perturbation induced potential will both be simultaneously projected under the targeted bonding cases. Our related coding technique has been compiled within the simple rotationally invariant DFT+U framework imbedded within the CASTEP source code (Vladimir et al., 1997). The C-2p orbital Hubbard U response is self-consistently performed based on the

Broyden-Fletcher-Goldfarb-Shannon (BFGS) geometry optimization algorithm. The PBE functional is chosen and related plane wave basis set cut-off energy is set at the 750 eV based on a Monkhost-Pack k-point mesh of 4×4×2. The ensemble DFT (EDFT) has been used for improving the electronic minimization to overcome the spurious spin-charge perturbation seen in density-mixing scheme (Marzari et al., 1997). The convergence tolerance of total energy calculation is determined at 5.0 x 10^{-7}eV/atom with ionic force minimization level of 0.001 eV/ Å by Hellmann-Feynman theorem.

The Pd, C, and H norm-conserving pseudopotentials are generated using the OPIUM code in the Kleinman-Bylander projector form (Kleinman et al., 1982), and the non-linear partial core correction for the Pd valence electrons (Louise et al., 1982) and a scalar relativistic averaging scheme (Grinberg et al., 2000) are selected to treat the spin-orbital coupling effect. We chose the (4*d*, 5*s*, 5*p*), (2*s*, 2*p*), (1s) states as the valence states of Pd, C, and H atoms respectively. The RRKJ method is chosen for the optimization of the pseudopotentials (Rappe et al., 1990).The Hubbard U parameters on the Pd-4d orbitals is self-consistently to be U_d=7.56eV.

Characterizations

Scanning electron microscopy (SEM) images were collected using an S-4800 field emission scanning electron microscope. Transmission electron microscopy (TEM), high resolution transmission electron microscopy (HRTEM) and EDX mapping results were carried out on a JEM-2100F electron microscope operating at 200 kV. X-ray diffraction (XRD) was conducted on a Japan Rigaku D/max-2500 rotation anode X-ray diffractometer using Cu Kα radiation (λ = 1.54178 Å). Raman spectra were obtained by e a Renishaw-2000 Raman spectrometer exploiting a 514.5 nm excitation laser source. And a Thermo Scientific ESCALab 250Xi instrument with monochromatic Al Kα X-ray radiation was used to perform the X-ray photoelectron spectroscope (XPS) measurement. Sub-ångström-resolution high-angle annular dark-field (FAADF) scanning transmission electron microscopy (STEM) images were obtained on aberration-corrected cubed FET Titan Cubed Themis G2 300 or JEM-ARM200F (JEOL, Tokyo, Japan) TEM/STEM operated at 200 kV with cold field-emission gun and double hexapole Cs correctors (CEOS GmbH, Heidelberg, Germany).

Electrochemical studies

All electrochemical experiments were performed using an electrochemical workstation (CHI. 660D, Shanghai CH. Instruments, China) with a typical three-electrode system. The as-prepared catalysts were used as working electrode; a graphite rod and saturated calomel electrode (SCE) was employed as the counter electrode and reference electrode, respectively. We used 0.5 M H_2SO_4 (saturated with H_2) as the electrolyte. Linear sweep voltammetry (LSV) measurements were conducted out at a scan rate of 1 mV s^{-1} and cyclic voltammograms (CV) measurements were performed within a range of -0.7 to 0 V at a scan rate of 100 mV s^{-1}. EIS data were gathered a frequency range from 0.1 to 100000 Hz at corresponding open circuit voltage. The chronoamperometric test result was carried out at a constant overpotential to reach an initial current density of 10 mA cm-2. All the potentials acquired were compensated by impedance and calibrated to the reversible hydrogen electrode (RHE).

Calculation of active sites and turn over frequency (TOF)

The TOF value of Pd^0/GDY can be obtained following the equation:

$$\mathrm{TOF} = \frac{\text{total hydrogen tunover per geometrica area}}{\text{active sites per geomtric area}}$$

The total hydrogen turnovers were calculated from the current density given from LSV curves in different overpotential according to the following equation:

total hydrogen tunovers

$$= \left(\mathrm{j}\frac{\mathrm{mA}}{\mathrm{cm}^2}\right)\left(\frac{1\ \mathrm{C/s}}{100\ \mathrm{mA}}\right)\left(\frac{1\ \mathrm{mol\ e^-}}{96485.3\ \mathrm{C}}\right)\left(\frac{1\ \mathrm{mol\ H_2}}{2\ \mathrm{mol\ e^-}}\right)\left(\frac{6.022\times10^{23}\ \mathrm{molecules\ H_2}}{1\ \mathrm{mol\ H_2}}\right)$$

$$= 3.12\times10^{15}\,\frac{\mathrm{H_2/s}}{\mathrm{cm}^2}\,\mathrm{per}\,\frac{\mathrm{mA}}{\mathrm{cm}^2}$$

Since the Pd^0/GDY fulfilled the maximum palladium atom efficiency, it was reasonable to assume that all the individual Pd atoms anchored on GDY could serve as active centers during HER process. Thus the active site can be calculated according to the ICP-MS result:

$$\text{active sites (Pd)} = \left(\frac{\text{mass loading (Pd)} \times \text{catalystloading per geometric area (g/cm}^2)}{\text{Pd Mw (g/mol)}}\right)\left(\frac{6.022\times10^{23}}{1\ \text{mol Pd}}\right)$$

$$= \left(\frac{0.2\%\times0.45\times10^{-3}(\mathrm{g/cm^2})}{106.42\ (\mathrm{g/mol})}\right)\left(\frac{6.022\times10^{23}}{1\ \text{mol Pd}}\right) = 5.1\times10^{15}\ \text{sites per cm}^2$$

The current density was obtained from LSV curve. Therefore, the TOF value was calculated according to the following equation:

$$\mathrm{TOF}_{\mathrm{Pd^0/GDY}} = \left(\frac{3.12\times10^{15}}{5.1\times10^{15}}\times j\right) = 0.612\times j$$

Calculation of mass loading

The mass activity can be calculated according to the equation:

$$\mathrm{j_{mass}} = \frac{\mathrm{j_{geometrical}}}{\mathrm{M_{loading}}}$$

in which $j_{\mathrm{geometrical}}$ is the geometrical current density directly obtained from LSV curve, while $\mathrm{M_{loading}}$ is the catalytically active Pd loading per geometric area calculated form ICP-MS result.

Calculation of double layer capacitance (C_{dl}) and electrochemical active surface area (ECSA)

The C_{dl} values are obtained based on the collected EIS data according to the following equation:

$$C_{dl} = \left[\frac{\mathrm{Q'}}{\left({R_S}^{-1} + {R'}^{-1}\right)^{1-n}}\right]^{(1/n)}$$

Where Rs is the uncompensated solution resistance; R' is the catalytic charge transfer resistance and Q' represents the influence of double layer capacitance. All these impendence parameters are listed in Table S2.

The ECSA values are collected from C_{dl} according to the equation:

$$\mathrm{ECSA} = \frac{C_{dl}}{C_s}$$

The specific capacitance (Cs) of the catalysts is generally considered to be 0.035 mF cm^{-2} in acidic working media according to peer recognition in reported studies.

Supplemental References

Clark, S. J., Segall, M. D., Pickard, C. J., Hasnip, P. J., Probert, M. I., Refson, K., and Payne, M. C. (2005). First principles methods using CASTEP. *Zeitschrift Fur* Kristallographie *220*, 567–570.

Grinberg, I., Ramer, N. J. and Rappe, A. M. (2000). Transferable relativistic dirac-slater pseudopotentials. Phys. Rev. B *62*, 2311.

Huang, B. (2016). Intrinsic deep hole trap levels in Cu_2O with self-consistent repulsive Coulomb energy. Solid State Commun. *230*, 49–53.

Huang B. (2016). Strong compensation hinders the p-type doping of ZnO: a glance over surface defect levels. Solid State Commun. *237*, 34–37.

Huang, B. (2017). The screened pseudo-charge repulsive potential in perturbed orbitals for band calculations by DFT+ U. *Phys.* Chem. Chem. Phys. *19*, 8008–8825.

Huang, B. (2016). 4f fine–structure levels as the dominant error in the electronic structures of binary lanthanide oxides. J. Comput. Chem. *37*, 825–835.

Kleinman, L. and Bylander, D. M. (1982). Efficacious form for model pseudopotentials. Phys. Rev. Lett. *48*, 1425.

Louie, S. G., Froyen, S. and Cohen, M. L. (1982). Nonlinear ionic pseudopotentials in spin-density-functional calculations. Phys. Rev. B *26*, 1738.

Marzari, N., Vanderbilt, D. and Payne, M. C. (1997). Ensemble density-functional theory for ab initio molecular dynamics of metals and finite-temperature insulators. Phys. Rev. Lett. *79*, 1337.

Rappe, A. M., Rabe, K. M., Kaxiras, E. and Joannopoulos, J. D. (1990). Optimized pseudopotentials. Phys. Rev. B *41*, 1227–1230.

Vladimir, I. A., Aryasetiawan, F. and Lichtenstein, A. I. (1997). First-principles calculations of the electronic structure and spectra of strongly correlated systems: the LDA+U method. J. Phys. Condens. Matter. *9*, 767–808.